NANO LETTERS
Letter
Cite This: Nano Lett. 2018, 18, 8035−8040
pubs.acs.org/NanoLett

Selected and Enhanced Single Whispering-Gallery Mode Emission from a Mesostructured Nanomembrane Microcavity

Ziao Tian,[†,‡] Shilong Li,[§] Suwit Kiravittaya,[∥] Borui Xu,[†] Shiwei Tang,[†] Honglou Zhen,[§] Wei Lu,[§] and YongFeng Mei*[,†]

[†]Department of Materials Science, State Key Laboratory of ASIC and Systems, Fudan University, 220 Handan Road, Shanghai 200433, China

[‡]State Key Laboratory of Functional Materials for Informatics, Shanghai Institute of Microsystem and Information Technology, Chinese Academy of Sciences, Shanghai 200050, China

[§]State Key Laboratory of Infrared Physics, Shanghai Institute of Technical Physics, Chinese Academy of Sciences, 500 Yutian Road, Shanghai 200083, China

[∥]Department of Electrical and Computer Engineering, Faculty of Engineering, Naresuan University, Taphoo, Muang, Phitsanulok 65000, Thailand

S *Supporting Information*

ABSTRACT: Quantum sciences are revolutionizing computing and communication technologies, in which single-photon emitters are the key components for creating strong quantum entanglement. Color centers in diamonds in coupled-cavity systems are considered great candidates for the efficient generation of quantum carriers over other solid-state emitters. Owing to the multi-mode nature of high quality factor (Q) diamond cavities, however, it is a grand challenge to the achievement of single photon emission with high rate and indistinguishability. To this end, a single-mode high-Q diamond cavity is highly desired. Here, we report a diamond mesostructured nanomembrane microcavity of a discrete rotational symmetry that selectively produces the desired single-mode emission in a broad spectrum. The strategic rolling up of a flexible diamond nanomembrane with aligned holes effectively defines the designed symmetry while maintaining the high-Q resonance through the whispering-gallery mode supported in the central hollow microcavity. The demonstrated diamond mesostructured microcavity features a distinct and enhanced single-mode emission, a step toward efficient quantum sources with designed positions or bands for quantum information technology.

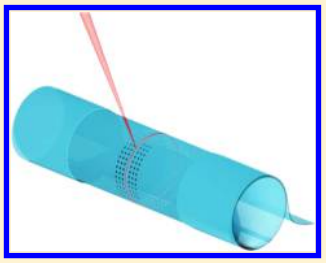

KEYWORDS: *Diamond, single mode, self-rolled up, self-alignment*

Advances in integrated photonic technologies have enabled the ability to generate, manipulate, and detect optical signals on a chip for both the classical and the quantum information sciences.[1−8] A variety of solid-state emitters including nanocrystals,[7] quantum dots,[8] and color centers[2−5] are available as the light source. The spontaneous emission spectrum from such a solid-state emitter typically consists of both the zero-phonon line (ZPL) and the phonon sideband because of the transparent solid matrix. Unfortunately, the ZPL that is of special interest for information applications has a relatively weaker intensity compared to the phonon sideband, especially at room temperature (RT). Strategically designed on-chip optical microcavities can offer potential solutions if specifically enhancing only the ZPL emission but suppressing emissions into phonon sidebands and other nonradiative decay channels.[4] Such ZPL emission can be strongly enhanced by whispering-gallery (WG) mode resonances in dielectric optical microcavities for their associated high quality factor (Q).[9−15] Due to their large volume compared to the effective wavelength, however, WG mode microcavities typically support multiple-modes oscillating simultaneously, which unfortunately boost the undesired phonon sidebands together with indistinct ZPL emission.

Origami, best known as the ancient art of paper folding, is the capability of a structure to fold or buckle without external manipulations and offers engineers novel ways to fabricate complex structures. Nowadays, origami-inspired 3D mesostructures with functional nanomembrane materials have enabled in a wide range of applications. In this Letter, using origami technology, we delicately render a diamond mesostructured microcavity with a discrete rotational symmetry to obtain a single WG mode ZPL emission with a high signal-to-noise ratio. The self-rolling-up of a diamond nanomembrane using strain-engineering and lift-off techniques precisely aligns the holes of different rolls to strategically define the discrete rotational symmetry for the diamond mesostructured microcavity, enabling distributed feedback to select the desired WG mode circulating inside the cavity. Such a strong modulation phase matches only the desired WG mode at the Bragg gap,[16] whereas all other WG modes experience non-coherent rigorous

Received: October 22, 2018
Published: November 14, 2018

DOI: 10.1021/acs.nanolett.8b04259
Nano Lett. 2018, 18, 8035−8040

scattering and thereby becoming suppressed, which, altogether, leads to enhanced single-mode emission from diamond without lasing.

The proposed single-mode microcavity along with its multiple-mode counterpart are depicted in Figure 1. In the multiple-mode cavity (a schematic of a multiple-mode tubular nanomembrane microcavity is shown in the inset of Figure 1a), the sub-wavelength-thin wall thickness h allows only localized optical field with the lowest radial mode index of $N = 1$, while the optical field can also be restricted with the fundamental axial mode index of $L = 1$ using a wavelength-scale axial barrier length of w. Unfortunately, it is impossible to further take the smallest azimuthal mode index $M = 1$ by simply shrinking the size of the cavity because of the large scattering loss by increased curvature. Figure 1a shows the schematic dispersion relation of resonant modes in the multiple-mode cavity; the regularly distributed WG modes with mode indices $\{N = 1, L = 1, \text{and } M \in \mathbf{N}^+\}$ are clear demonstrated, showing highly packed peaks even in a narrow emission spectrum (Figure 1b). The single-mode cavity in our work consists of periodic hole arrays mirror-symmetrically distributed on both sides of a tubular nanomembrane microcavity (see the inset of Figure 1b). In a similar design, in the multiple-mode counterpart, only the resonant modes with the lowest mode indices $N = 1$ and $L = 1$ are allowed in the single-mode cavity. In contrast, further restriction imposed by the discrete rotational symmetry by the periodic holes gives rise to a single longitudinal mode with $M = m_0$, where m_0 is the grating order of the introduced hole array along the circumference. Therefore, a single WG mode with mode indices $\{N = 1, L = 1, \text{and } M = m_0\}$ is defined in the dispersion diagram (Figure 1a) and thus provides a single peak in the emission spectrum (Figure 1b). Note that such the discrete rotational symmetry cannot be imposed on WG modes in an in-plane manner without breaking the mirror symmetry of the double-sided hole arrays. Consequently, a vertically aligned tubular nanomembrane microcavity would be the only possibility to simultaneously support these structural symmetries. However, it remains a grand challenge to construct three-dimensional distributed holes onto a micro-scale vertical structure. Examples of both multiple-mode (left panel and middle panel) and single-mode (right panel) cavities using rolled-up nanotechnology are shown in Figure 1c. Compared to the tube cavity (left panel), the bottle-like tubular cavity (middle panel) has an axial confinement due to its parabolic lobe and thus exhibits sharp multiple resonance peaks. Replacing the lobe by periodic hole arrays, a single resonance peak is obtained the resultant tube cavity (right panel).

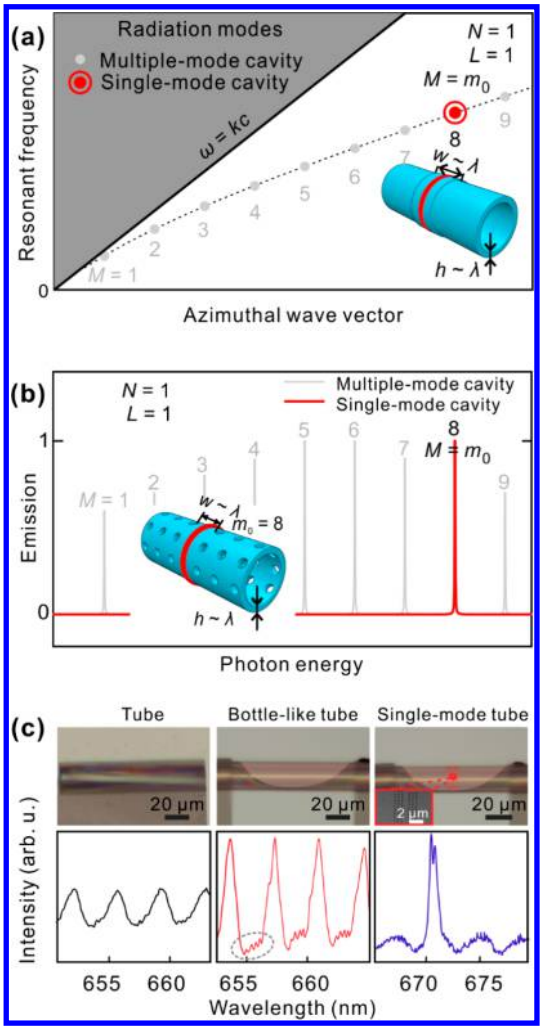

Figure 1. Design of single WG mode optical microcavities. (a) Dispersion diagrams of optical modes in the multiple-mode (light gray dots) and single-mode (red dot) cavities. Inset shows schematic of a multiple-mode tubular nanomembrane microcavity. Only modes indexed $N = 1$ and $L = 1$ are allowed due to the wavelength-scale thickness h and axial barrier length w, respectively. The mode index M is not restricted because of the translational rotational symmetry. Typical optical-field distribution is indicated by the thick red line. (b) Emission spectra for the multiple-mode (light gray line) and single-mode (red line) cavities. The spectral line width is exaggerated for clarity. Inset shows schematic of a single-mode tubular nanomembrane microcavity. The presence of periodic hole arrays provides a discrete rotational symmetry for only the WG mode with $M = m_0$, where m_0 is the grating order of hole array along the circumference. Optical-field distribution is shown by the thick red line. (c) Examples of both multiple-mode (left panel and middle panel) and single-mode (right panel) cavities using rolled-up nanotechnology. The gray dashed circle indicates a series of subpeaks, known as axial modes.

The single WG mode microcavity is realized based on the so-called rolled-up nanotechnology.[17,18] The fabricated rolled-up microcavity shows a distinctly single WG mode peak over the entire emission spectrum. The experimental result is confirmed by numerical simulations based on the finite element method (FEM). Tailoring of the single-mode emission is carried out to demonstrate the wavelength-tuning ability of the rolled-up microcavity. Diamond, which is known as "the ultimate engineering material",[2,19] is used to maintain an enough mechanical strength of the material nanomembrane perforated with punch-through holes before the rolling. Figure 2a illustrates the fabrication process of rolled-up diamond single-mode microcavities (see Part 1 in the Supporting Information for more details). It combines two competing principles, i.e., both top-down and bottom-up approaches. Based on the top-down approach, a diamond nanomembrane was patterned by the standard electron-beam lithography and etching procedures. The pattern consists of a U-shaped mesa perforated with periodic hole arrays (Figure 2b,c). The U-shaped mesa is designed to raise the center part of the resultant rolled-up microcavity so that the scattering loss of light caused by the underneath substrate can be avoided, while the periodic hole array defines the discrete rotational symmetry for the sake of single-mode resonance and constitutes a phase-modulated

DOI: 10.1021/acs.nanolett.8b04259
Nano Lett. 2018, 18, 8035−8040

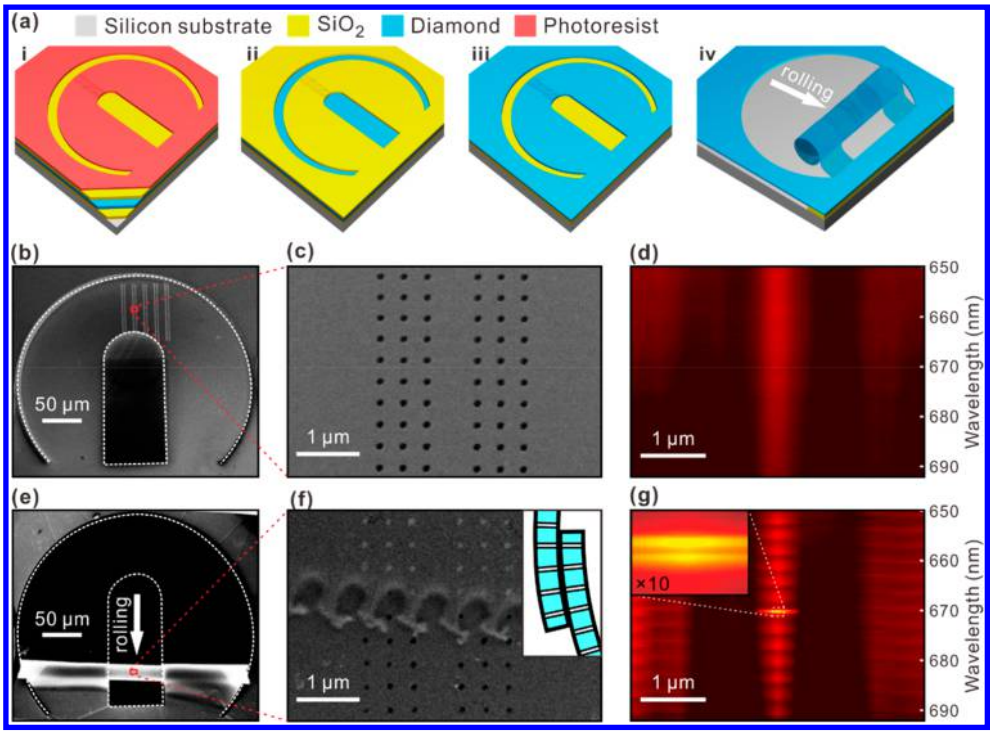

Figure 2. Experimental realization of on-chip single WG mode optical microcavities using rolled-up nanotechnology. (a) Steps to fabricate the rolled-up microcavities from a diamond nanomembrane. There are four main steps: (i) patterning of the top photoresist layer, (ii) pattern transferring to the SiO_2 hard mask layer, and (iii) sequentially to the diamond nanomembrane layer, and (iv) removing of the underneath SiO_2 sacrificial layer. (b) Scanning electron microscopy (SEM) image of the nanopatterned diamond nanomembrane, and (c) its enlarged view showing the array of holes. (d) PL mapping for the nanopatterned diamond nanomembrane. (e) SEM image of the rolled-up diamond microcavity, and (f) its enlarged view showing the overlap of the hole array. Inset: schematic of the nanomembrane cross-section where patterned holes are aligned. (g) PL mapping for the rolled-up diamond microcavity. Inset: magnified (10×) PL mapping of the confinement-enhanced mode. Note that the pseudocolor map is adjusted to enhance the other weak mode peaks while the main peak intensity is highly saturated.

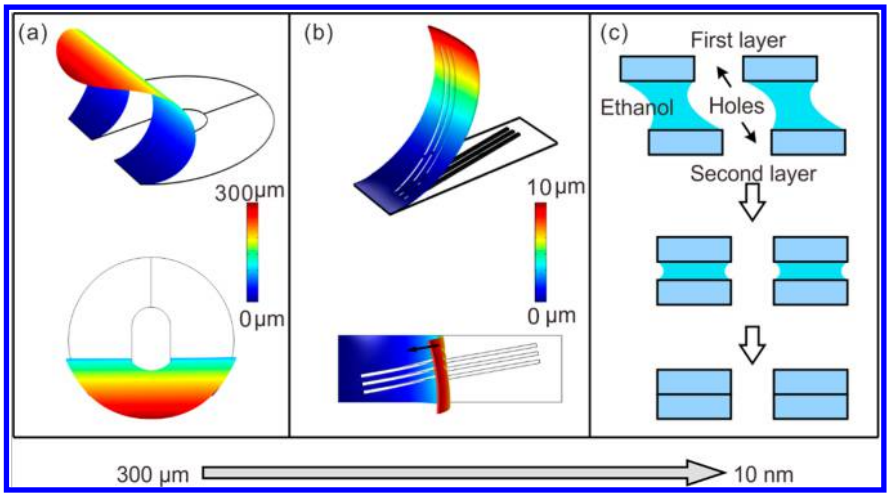

Figure 3. Directional control of the rolling process by three-step self-alignment. (a) 3D perspective (high) and top views (low) of the considered bilayer film after releasing the initial strain. Note that a bilayer film consisting of the upper layer with a tensile strain and the lower layer with a compressive strain, instead of a single-layer diamond membrane used in the experiment, is used in the simulations. (b) A 3D-perspective view (high) of the result from the simulations of the nanopatterned films and a top view (low) from the same simulations. (c) Schematic of the self-alignment using surface tension.

strip waveguide. Combined with the bottom-up approach, the patterned diamond nanomembrane can be self-assembled into a microscale vertically aligned tubular structure due to the release of residual strain within the nanomembrane (Figure 2e,f). As a result, the phase-modulated strip waveguide is self-enclosed, and a discrete rotational symmetry is spontaneously emerged. Interestingly, the nanopatterned holes are self-aligned (see the inset of Figure 2f). This self-alignment will be discussed in Figure 3.[20] Altogether, by combining the two approaches to unfold the full potential of nanotechnology, a microscale vertical structure with three-dimensional distributed holes is realized in a reproducible and controllable manner.

Spectral and spatial resolved photoluminescence (PL) measurements on the fabricated diamond structure were

DOI: 10.1021/acs.nanolett.8b04259
Nano Lett. 2018, 18, 8035−8040

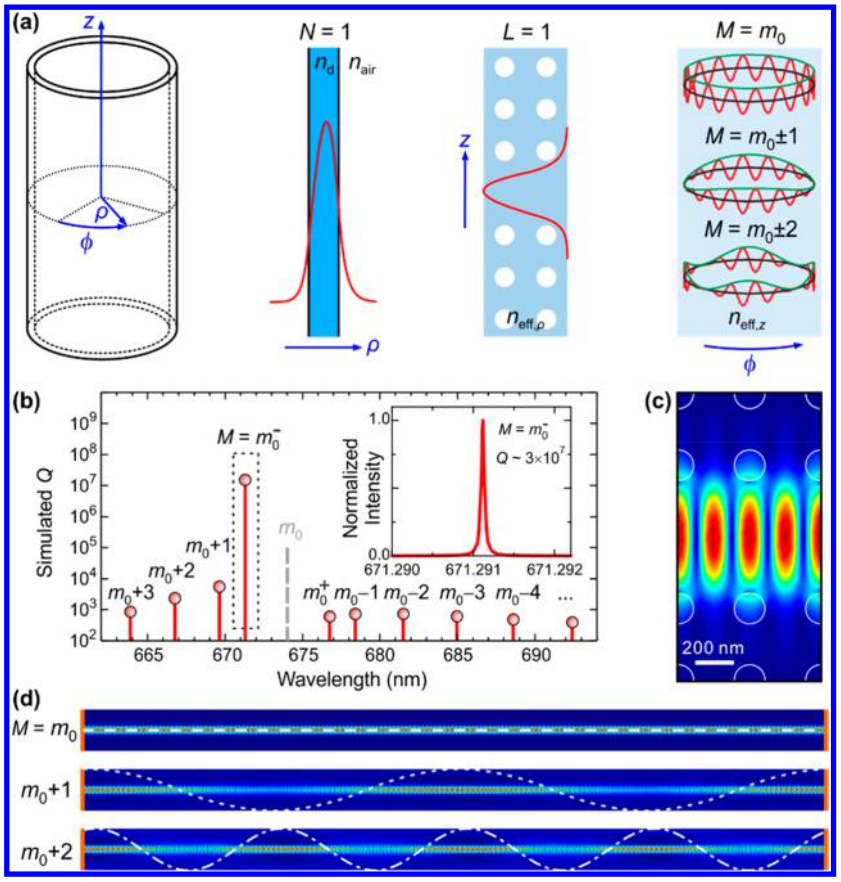

Figure 4. Theoretical modeling and numerical simulations of single WG mode optical microcavities based on periodic boundaries. (a) Sketches of a rolled-up microcavity under the ring approximation and the corresponding electric-field components indicated by the red lines along the radial ρ, axial z, and azimuthal ϕ direction, respectively. The green lines show also the envelope function for clarity. See the main text for the meaning of these effective refractive indices. (b) Simulated Q of each mode showing a single high-Q peak along with several broad WG mode peaks. Inset: emission spectrum for the mode M = m_0^-. (c) The electric field distributions for the confined mode of $L = 1$ in two unit cells and (d) the first three azimuthal modes ($M = m_0$, $m_0 + 1$, and $m_0 + 2$) in the (ϕ, z) two-dimensional plane. The envelopes of the periodically distributed electric fields are shown in dashed lines, dotted lines, and dash−dotted lines for the modes $M = m_0$, $m_0 + 1$, and $m_0 + 2$, respectively.

performed at RT. A typical PL spectrum consists of a single sharp peak over a large range of wavelengths (see, e.g., Figure 2g), and the side mode suppression ratio can reach up to approximately 12 dB, indicating that the diamond structure is a robust single-mode microcavity. Moreover, the Q of the single peak is high (~2500), which is not only comparable to the highest value of 5400 in rolled-up SiO_2 multiple-mode optical microcavities operated in emission mode[21−23] but also higher than the values reported for polycrystalline diamond multiple-mode microstructures in the visible spectral range.[24,25] In addition to the strong temporal confinement of light characterized by the high Q, the single mode can produce a strong spatial confinement for light as well. Distance between the patterned holes along the axial z direction can be designed to provide the spatial confinement in a deterministic and controllable manner. Panels d and g of Figure 2 show the PL mappings expanded by the axial position and the wavelength before and after the rolling, respectively. As can be clearly visible from these PL mappings, both strong temporal and spatial confinements for a single resonant mode are enabled in the rolled-up diamond microcavities.

As shown in the inset of Figure 2g, the single sharp peak in fact consists of a nearly degenerate pair of modes, which is the mode splitting and has been observed experimentally[26] in rolled-up multiple-mode optical microcavities. Several numerical studies on the mode splitting have been reported as well[26−28] and show that the split WG mode pairs arise from the local structural singularities owing to the overlap of layers in a rolled-up structure.[28]

Figure 2f shows that the nanopatterned holes are self-aligned exactly. This self-alignement is attributed to three-step self-alignment, as shown in Figure 3. According to previous reports, the directional rolling can be controlled by anisotropic mechanical property and geometry design of pre-rolling nanomembranes. The latter one can be applied in isotropic materials for directional rolling due to the minimization of the total elastic energy. However, the directional control of the rolling process in nanoscale is still challenging to achieve. In this part, we demonstrated that the nanopatterned holes array is exactly aligned in nanoscale by three-step self-alignment. First, a symmetric rolling of the film to fixed boundary is observed in the large scale (about 300 μm) due to the symmetric circular pattern as shown in Figure 3a. Next, the rolling direction is further controlled by the nanopattern on the films. Next, we further demonstrate that the rolling direction can be well-controlled by the nanopatterned holes. In the realistic experiments, we have a large number of nanopatterned holes aligned perpendicular to the fixed boundary of the large pattern. However, to demonstrate the control of the rolling by the patterned holes, we have performed a simplified additional

DOI: 10.1021/acs.nanolett.8b04259
Nano Lett. 2018, 18, 8035−8040

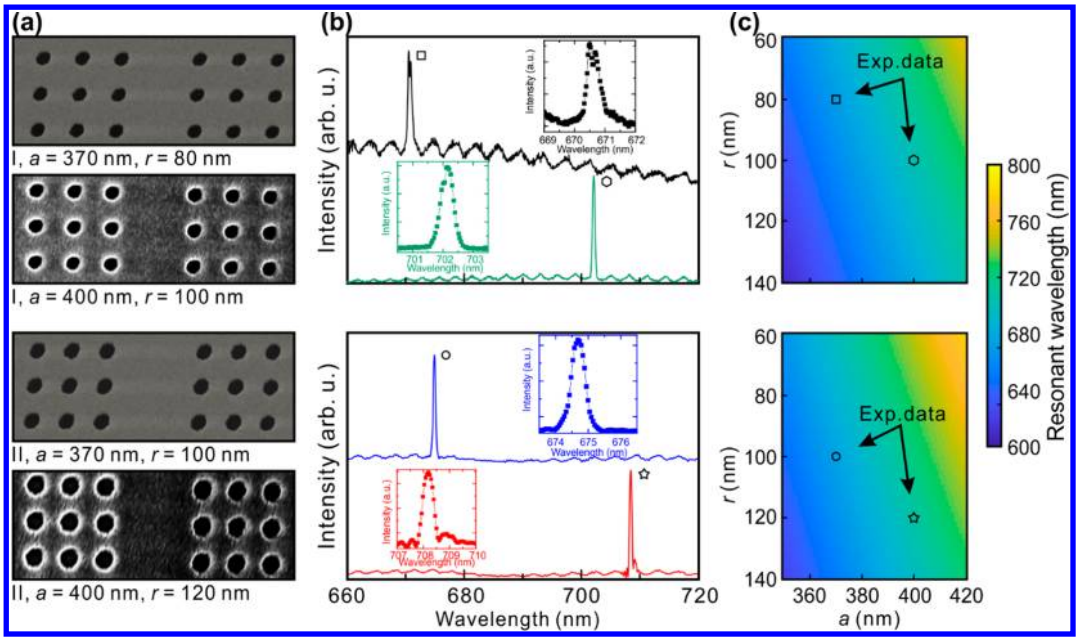

Figure 5. Tailoring of the single WG mode in rolled-up diamond microcavities. (a) SEM images of rolled-up microcavities with one (I) or two (II) missing rows of the holes fabricated with different hole period a and radius r, (b) the corresponding PL spectra showing single-mode emission at different wavelengths, and (c) the calculated dependency of the resonant wavelength on the number of missing rows, hole period a, and radius r. In panels b and c, different symbols are used to mark the resonant peaks.

simulation by using array of rectangular holes. Figure 3b shows the result from the simulation from the patterned films. These holes are tiled by 10 degrees from the edge of the film. The directional control of the rolling in the patterned film is clearly observed when the simulation results are reviewed from top view. Because, in the realistic experiments, we have nanopatterned hole aligned perpendicular to the fixed boundary of the large pattern, we are confident that the rolling direction is well-controlled by both the large scale pattern (via the fixed boundary) and nanopatterned holes (via the alignment of the hole). Finally, surface tension has also been used to carry out self-alignment in nanometer scale (10 nm).[20] Actually, the capillary-driven self-alignment using droplets or capillary self-assembly is extensively investigated for 3D microelectronics. This method aims to be an alternate approach to the pick and place approach. In our case, we assume that the surface tension forces associated with capillary pinning create restoring forces and torques that tend to bring the moving part into alignment in nanoscale. The basic sequence is illustrated in Figure 3c. During the rolling of more than one rotation, the holes in each layer do overlap with those of neighboring layers. Next, the surface tension of the ethanol aligns the holes. After evaporation of the ethanol, two parts have been bounded to each other. More details see additional evidence from numerical simulations on the directional control of the rolling in part 2 of the Supporting Information.

To get a deeper understanding of the single-mode property in the rolled-up diamond microcavities, a theoretical model based on rolled-up multiple-mode microcavities[17] is investigated in conjunction with the coupled-wave theory[16] (see part 3 in the Supporting Information for more details). In short, as shown in Figure 4a, light with a single wavelength near the Bragg reflection is fully quantized with the deterministic mode-index set $\{N = 1, L = 1, \text{and } M = m_0\}$ in the rolled-up diamond microcavities, as we expected. Numerical simulations were carried out to verify the experimental observation and theoretical analysis. In the simulations, the rolled-up diamond microcavity is treated as a periodic planar nanomembrane with a length of πd by applying the periodic boundary condition on its two ends. In addition, only in-plane electric fields (TM mode) in the (ϕ, z) two-dimensional plane with a refractive index of $n_{\text{eff},\rho}$ for the $N = 1$ mode were calculated. The simulation results are summarized in Figure 4b, along with the typically obtained field profile in Figure 4c for $L = 1$ and Figure 4d for $M = m_0$, $m_0 + 1$, and $m_0 + 2$. The good agreement between the experiments and the simulations confirms that the observed single-mode confinement-enhanced resonant peak results from the combination of a phase-modulation mechanism and a WG resonance for light in the rolled-up diamond microcavities.

For most of the applications using single-mode optical microcavities, matching the single mode into the desired wavelength range is highly desired. Tailoring the single WG mode in rolled-up diamond microcavities was thus performed by varying the nanopatterned hole array before the rolling, and the results are summarized in Figure 5. All of the rolled-up nanomembranes have the same range of diameter (20−30 μm). As can be seen from Figure 5, by varying both the hole radius and period as well as the number of missing hole rows, the position of the single WG mode can be tailored over a wide wavelength range. Part 3 of the Supporting Information presents the fitting of the experimentally observed peaks based on the coupled-wave theory. The coupled refractive index (a fitting parameter) can qualitatively explain the effects of the hole period and radius on the mode position. The wide wavelength tuning range demonstrated here (Figure 5) is sufficient for the many purposes of any specific physical demonstration. Further efforts on this aspect should be undertaken in the future.

In conclusion, we have proposed and demonstrated a single-mode confinement-enhanced microcavity by combining the advantages of phase-modulation mechanism and WG reso-

DOI: 10.1021/acs.nanolett.8b04259
Nano Lett. 2018, 18, 8035−8040

nance. This concept is realized by rolling up nanopatterned diamond nanomembranes, in which the self-alignment of the patterned holes on the overlapped part is observed in a notable way. The periodic hole array defines the properties of the single WG mode, in which the confinement of light is enhanced. The experimental result is confirmed by the numerical simulations. Although we report here the realization of single-mode confinement-enhanced microcavities, the presented experimental technique can be used for other nanopatterned structures such as photonic crystal waveguides and microcavities.

■ ASSOCIATED CONTENT

Supporting Information

The Supporting Information is available free of charge on the ACS Publications website at DOI: 10.1021/acs.nanolett.8b04259.

Detailed information about the fabrication, optical measurements, and theoretical models; numerical simulations with finite element method on the directional control of the rolling process; and information on the coupled-wave theory (PDF)

■ AUTHOR INFORMATION

Corresponding Author

*E-mail: yfm@fudan.edu.cn.

ORCID

YongFeng Mei: 0000-0002-3314-6108

Author Contributions

Z.T. and S.L. contributed equally. Y.M. conceived the concept. Z.T., under the supervision of Y.M., carried out the fabrications. Z.T., B.X., and S.T. carried out the characterizations of the diamond nanomembranes and 3D structures. S.L., under the supervision of H.Z. and W.L., performed the theoretical modeling and numerical simulations. S.L. and S.K. co-wrote the manuscript. All authors discussed the results and commented on the manuscript.

Notes

The authors declare no competing financial interest.

■ ACKNOWLEDGMENTS

This work is supported by the Natural Science Foundation of China (grant nos. 51322201 and U1632115), Science and Technology Commission of Shanghai Municipality (grant no. 17JC1401700), the National Key Technologies R&D Program of China (grant no. 2015ZX02102-003), and the Changjiang Young Scholars Program of China. S.K. acknowledges the Fudan Fellow scholarship and the financial support from the Research Chair Grant, the National Science and Technology Development Agency (NSTDA), Thailand. S.L. acknowledges the financial support of the International Postdoctoral Exchange Fellowship Program (grant no. 20170010). Part of the experimental work has been carried out in Fudan Nanofabrication Laboratory. We also thank Prof. Zengfeng Di for fruitful discussion.

■ REFERENCES

(1) Beveratos, A.; Brouri, R.; Gacoin, T.; Villing, A.; Poizat, J.-P.; Grangier, P. *Phys. Rev. Lett.* **2002**, *89*, 187901.

(2) Lončar, M.; Faraon, A. *MRS Bull.* **2013**, *38*, 144−148.

(3) Babinec, T. M.; Hausmann, B. J. M.; Khan, M.; Zhang, Y.; Maze, J. R.; Hemmer, P. R.; Lončar, M. A. *Nat. Nanotechnol.* **2010**, *5*, 195−199.

(4) Faraon, A.; Barclay, P. E.; Santori, C.; Fu, K-M. C.; Beausoleil, R. G. *Nat. Photonics* **2011**, *5*, 301−305.

(5) Riedrich-Möller, J.; Kipfstuhl, L.; Hepp, C.; Neu, E.; Pauly, C.; Mücklich, F.; Baur, A.; Wandt, M.; Wolff, S.; Fischer, M.; Gsell, S.; Schreck, M.; Becher, C. *Nat. Nanotechnol.* **2012**, *7*, 69−74.

(6) O'Brien, J. L.; Furusawa, A.; Vučković, J. *Nat. Photonics* **2009**, *3*, 687−695.

(7) Priolo, F.; Gregorkiewicz, T.; Galli, M.; Krauss, T. F. *Nat. Nanotechnol.* **2014**, *9*, 19−32.

(8) He, Y.-M.; He, Y.; Wei, Y.-J.; Wu, D.; Atatüre, M.; Schneider, C.; Hofling, S.; Kamp, M.; Lu, C.-Y.; Pan, J.-W. *Nat. Nanotechnol.* **2013**, *8*, 213−217.

(9) Vahala, K. J. *Nature* **2003**, *424*, 839−846.

(10) Aoki, T.; Dayan, B.; Wilcut, E.; Bowen, W. P.; Parkins, A. S.; Kippenberg, T. J.; Vahala, K. J.; Kimble, H. J. *Nature* **2006**, *443*, 671−674.

(11) Alton, D. J.; Stern, N. P.; Aoki, T.; Lee, H.; Ostby, E.; Vahala, K. J.; Kimble, H. *Nat. Phys.* **2011**, *7*, 159−165.

(12) Armani, A. M.; Kulkarni, R. P.; Fraser, S. E.; Flagan, R. C.; Vahala, K. J. *Science* **2007**, *317*, 783−787.

(13) Zhu, J.; Ozdemir, S. K.; Xiao, Y.-F.; Li, L.; He, L.; Chen, D.-R.; Yang, L. *Nat. Photonics* **2010**, *4*, 46−49.

(14) Shao, L.; Jiang, X.-F.; Yu, X.-C.; Li, B.-B.; Clements, W. R.; Vollmer, F.; Wang, W.; Xiao, Y.-F.; Gong, Q. *Adv. Mater.* **2013**, *25*, 5616−5620.

(15) Baaske, M. D.; Foreman, M. R.; Vollmer, F. *Nat. Nanotechnol.* **2014**, *9*, 933−939.

(16) Kogelnik, H.; Shank, C. V. *J. Appl. Phys.* **1972**, *43*, 2327−2335.

(17) Kipp, T.; Welsch, H.; Strelow, Ch.; Heyn, Ch.; Heitmann, D. *Phys. Rev. Lett.* **2006**, *96*, 077403.

(18) Songmuang, R.; Rastelli, A.; Mendach, S.; Schmidt, O. G. *Appl. Phys. Lett.* **2007**, *90*, 091905.

(19) Aharonovich, I.; Greentree, A. D.; Prawer, S. *Nat. Photonics* **2011**, *5*, 397−405.

(20) Mastrangeli, M.; Zhou, Q.; Sariola, V.; Lambert, P. *Soft Matter* **2017**, *13*, 304−327.

(21) Böttner, S.; Li, S.; Trommer, J.; Kiravittaya, S.; Schmidt, O. G. *Opt. Lett.* **2012**, *37*, 5136−5138.

(22) Ma, L. B.; Li, S. L.; Fomin, V. M.; Hentschel, M.; Götte, J. B.; Yin, Y.; Jorgensen, M. R.; Schmidt, O. G. *Nat. Commun.* **2016**, *7*, 10983.

(23) Yin, Y.; Li, S. L.; Böttner, S.; Yuan, F. F.; Giudicatti, S.; Naz, E. S. G.; Ma, L. B.; Schmidt, O. G. *Phys. Rev. Lett.* **2016**, *116*, 253904.

(24) Rath, P.; Ummethala, S.; Nebel, C.; Pernice, W. H. P. *Phys. Status Solidi A* **2015**, *212*, 2385−2399.

(25) Tian, Z.; Zhang, L.; Fang, Y.; Xu, B.; Tang, S.; Hu, N.; An, Z.; Chen, Z.; Mei, Y. *Adv. Mater.* **2017**, *29*, 1604572.

(26) Strelow, Ch.; Schultz, C. M.; Rehberg, H.; Sauer, M.; Welsch, H.; Stemmann, A.; Heyn, Ch.; Heitmann, D.; Kipp, T. *Phys. Rev. B: Condens. Matter Mater. Phys.* **2012**, *85*, 155329.

(27) Hosoda, M.; Shigaki, T. *Appl. Phys. Lett.* **2007**, *90*, 181107.

(28) Fang, Y.; Li, S.; Mei, Y. *Phys. Rev. A: At., Mol., Opt. Phys.* **2016**, *94*, 033804.

DOI: 10.1021/acs.nanolett.8b04259
Nano Lett. 2018, 18, 8035−8040